Estuarine, Coastal and Shelf Science 293 (2023) 108487

Contents lists available at ScienceDirect

Estuarine, Coastal and Shelf Science

journal homepage: www.elsevier.com/locate/ecss

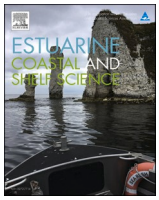

ENSO and NAO linkages to interannual salinity variability in north central Gulf of Mexico estuaries through teleconnections with precipitation

Gregg A. Snedden

U.S. Geological Survey, Wetland and Aquatic Research Center, Baton Rouge, LA, USA

A B S T R A C T

Though the importance of Earth's internal climate modes such as the El Niño-Southern Oscillation (ENSO) and the North Atlantic Oscillation (NAO) to regional-scale climate variability is well recognized, the degree to which these oscillations are reflected by spatio-temporal salinity variability over interannual timescales in estuaries is less understood. Here an 11-year continuous salinity monitoring dataset spanning 223 stations across Louisiana's coastal wetlands along the northern Gulf of Mexico is examined with empirical orthogonal function (EOF) analysis to identify dominant modes of interannual variability in the salinity field. The first EOF mode accounts for 72% of the variance in the salinity field and captures a domain-wide pattern where salinities vary in-phase through space in response to local precipitation anomalies occurring in the vicinity of the study area. This local precipitation anomaly is positively correlated with ENSO (Nino3.4 index), consistent with the El Niño – wet (La Niña – dry) precipitation teleconnection that is prevalent throughout the northern Gulf of Mexico coast. The second EOF mode, which accounts for 13% of the variance in the salinity field, is expressed primarily in the marshes across the lower reaches of the Mississippi River deltaic plain (MRDP). EOF2 is anticorrelated with annual Mississippi River discharge anomaly such that salinities in the lower MRDP decrease as discharge increases, pointing to enhanced advection of fresh river plume waters over the shelf into the estuary via estuary-ocean exchange during years of anomalously high river discharge. Mississippi River discharge anomaly is positively correlated with the NAO at a one-year time lag, through a teleconnection with precipitation throughout much of the central region of the Mississippi River drainage basin. Together, these findings indicate that most of the interannual salinity variability across Louisiana's coastal wetlands can be linked to climate variability through teleconnections with precipitation. Incorporating these dynamics into restoration planning, monitoring, and adaptive management efforts may help constrain background environmental variation and better isolate restoration effects.

1. Introduction

Understanding drivers of salinity regimes in estuaries and coastal wetlands is critical to ecosystem management and restoration, as salinity is an important determinant of ecosystem production (Wilber, 1992; van der Molen and Perissinotto, 2011; Mace and Rozas, 2017; Janousek et al., 2020), biodiversity (Latham et al., 1994; Maes et al., 1998; Winder and Sommer, 2012; Telesh et al., 2013), and function (Morris et al., 1978; Nowicki, 1994; van de Broek et al., 2016; Wang et al., 2018). In addition to these direct ecosystem effects of salt concentrations in estuarine waters, the balance between seaward advection of salt by river flow and landward salt transport by dispersive processes regulates circulation and stratification which, in turn, can impact ecosystem processes such as phytoplankton production (Malone et al., 1988) and larval nekton transport (Norcross and Shaw, 1984; Dong et al., 2007; Meerhoff et al., 2015). Salinity also influences water quality (Howarth et al., 2011; Murphy et al., 2011), and as such can serve as an important indicator of nutrients, heavy metals, suspended sediments, and dissolved oxygen in coastal waters (MacCready and Geyer, 2001; Wei et al., 2016).

Estuarine salinity is strongly influenced by the magnitude, frequency, duration, and timing of episodic freshwater inflows and the way these inflows interact with saline shelf waters. These interactions are shaped by a variety of atmospheric and oceanic mechanisms that occur over a broad range of time scales. These mechanisms include advection by the lunar tide (Ralston et al., 2010; Xu et al., 2019), fortnightly variations caused by changes in tidal amplitude over the spring-neap cycle (de Miranda et al., 1998; Lerczak et al., 2006), wind-forced estuary-ocean exchange (Garvine, 1985; Sanford and Boicourt, 1990; Wong and Moses-Hall, 1998), and seasonal variations in local precipitation and runoff (Wong, 1995; Ralston et al., 2008).

Over interannual time scales, salinity in estuaries and coastal wetlands can vary with year-to-year fluctuations in river discharge and coastal sea level (Hilton et al., 2008; Murphy et al., 2011). In the Delaware Estuary, long-term positive salinity trends have been linked to sea-level rise (Ross et al., 2015). In many regions, teleconnections between these variables and Earth's internal climate modes have been observed. For example, the North Atlantic Oscillation (NAO) is inversely correlated with Connecticut River discharge, and positively correlated with salinity in Long Island Sound (Whitney, 2010). Estuarine salinity in

E-mail address: sneddeng@usgs.gov.

https://doi.org/10.1016/j.ecss.2023.108487
Received 15 June 2023; Received in revised form 1 September 2023; Accepted 5 September 2023
Available online 6 September 2023
0272-7714/Published by Elsevier Ltd.

Patos Lagoon (Fernandes et al., 2002; Bitencourt et al., 2020), Tampa Bay (Schmidt and Luther, 2002), and along the Texas Gulf Coast (Tolan, 2007) is inversely correlated with the Nino3.4 index, such that El Niño events are associated with negative salinity anomalies. These year-to-year salinity oscillations can impose cascading impacts to water quality (Tominack et al., 2020) and estuarine food webs (Garcia et al., 2001; Stenseth et al., 2002; Piazza et al., 2010; Cloern et al., 2016).

In coastal Louisiana, interannual variation in salinity has been linked to variation in fisheries productivity (Rozas and Minello, 2011; La Peyre et al., 2016), distribution and abundance of submerged aquatic vegetation (DeMarco et al., 2018), composition of phytoplankton communities (Mize and Demcheck, 2009), and benthic biogeochemical transformations (Seo et al., 2008). Additionally, interannual salinity fluctuations have been linked to changes in emergent marsh vegetation community zonation (Visser et al., 2002), where widespread transitions from oligohaline to mesohaline communities were observed following a two-year extreme drought. During the same time period, widespread dieback in coastal salt marshes dominated by the perennial marsh grass *Spartina alterniflora* occurred across the Mississippi River deltaic plain (McKee et al., 2004). Even subtle changes in salinity can markedly impact the performance of wetland plants common to coastal Louisiana (Willis and Hester, 2004; Spalding and Hester, 2007; Snedden et al., 2015), where decreased belowground production resulting from excessive salinity can lead to decreased organic matter accumulation and accretion, thus impairing the landscape's ability to maintain its vertical position in a rising tidal frame and placing its sustainability in question.

The tidal wetlands of Louisiana comprise nearly two-thirds of those in the Gulf of Mexico, and more than half of those found in the conterminous United States (Couvillion et al., 2017; Windham-Meyers et al., 2018)), yet 90% of the nation's coastal marsh loss occurs in Louisiana (Steadman and Dahl, 2008). It follows that the nearly $50B in ecosystem services the region provides annually in the form of water supply, water quality mitigation, storm surge protection, commercial navigation routes and ports, seafood landings, and recreation (Herrera et al., 2019), face imminent disruption. Beyond these ecosystem services, nearly 30% of the nation's annual oil production and 19% of its gas production move through pipelines in Louisiana's coastal zone that are not designed for the high wave-energy regimes that would prevail should the protection provided by the region's coastal wetlands be reduced or eliminated (Laska et al., 2005). Carbon burial rates in these wetlands – which are inversely correlated with salinity (Baustian et al., 2017) – exceed 4 Tg yr^{-1}, and account for up to 20% of the total global rate (Baustian et al., 2021). Thus, a significant global carbon sink is in jeopardy if current rates of wetland loss continue unabated. A globally unprecedented $50–100B, 50-yr ecosystem restoration effort is currently underway in coastal Louisiana (Peyronnin et al., 2013) and understanding how Earth's internal climate modes – through teleconnections with local- and Mississippi River drainage basin-scale precipitation – may impact year-to-year salinity variability will be a critical component for successful adaptive management of this restoration effort over the medium term (Steyer et al., 2003). Additionally, understanding these dynamics can inform predictions of how climate and land-use change may impact the long-term sustainability of this important landscape and the ecosystem services and energy security it provides to the region and to the world.

This study examines spatial-temporal variation of salinity measured at 223 stations over 11 years under Louisiana's Coastwide Reference Monitoring System (CRMS; (Deepwater Horizon Natural Resource Damage Assessment Trustees, 2022). Empirical orthogonal function (EOF) analysis is applied to identify dominant modes of variability in the dataset, and linkages between these dominant modes and geophysical forcing functions are explored. Correspondence between these forcing functions and various climate modes over several decades is then examined to identify linkages between the relevant climate modes and spatiotemporal salinity patterns across Louisiana's expanse of coastal wetlands.

2. Methods

2.1. Study area

The Louisiana Gulf Coast contains nearly 15,000 km^2 of marshes, swamps, and other lowland habitat (Fig. 1) that flank the northern Gulf of Mexico (GOM) coast and form a continuum of vegetation community types that largely reflect the landscape's long-term salinity regime (Snedden, 2019). The landscape can be divided into two primary regions – the Mississippi River deltaic plain (MRDP) and the Chenier Plain (LCP). The wetlands of the MRDP along eastern coastal Louisiana (east of 92°W longitude) reside atop Holocene sediment deposits that are products of the 3.2M km^2 Mississippi River drainage basin and roughly 8000 years of river avulsion events near the river's mouth. Along much of the MRDP west of the mouth of the Mississippi River, estuary-ocean exchange occurs primarily through a multitude of tidal passes situated between barrier islands. The LCP along western coastal Louisiana (west of 92°W longitude) was also formed with terrigenous sediments from the Mississippi River drainage basin, but after they were discharged to the northern GOM, subsequently transported to the region by the westward coastal current along the northern GOM shelf, and then reworked against the coast through wave action (Byrne et al., 1959; Gould and McFarlan, 1959). Ridges (or cheniers) and levees are common features of the LCP, and water exchange between LCP wetlands and the northern GOM is often inhibited by these features and occurs largely through a few narrow inlets incised through the ridges. Runoff from local precipitation over south Louisiana is a large source of fresh water for the coastal wetlands, delivered via a series of small rivers (blue lines, Fig. 1; see Supplementary Table S1). The Mississippi River and its distributary, the Atchafalaya River (brown lines, Fig. 1), are additional sources of fresh water to Louisiana's coastal wetlands. Because the Mississippi/Atchafalaya River system is largely leveed for flood control and commercial navigation, its fresh water reaches the coastal wetlands primarily either through tidal exchange after it is discharged into the GOM, or through the Gulf Intracoastal Waterway (red line, Fig. 1), which conveys Atchafalaya River flows east and west from the confluence of the two waterways (Swarzenski, 2003). It is important to note that the presence of flood-control levees along the flanks of the lower Mississippi River impedes runoff of local precipitation into the river itself and as such, the response of Mississippi and Atchafalaya River discharge to local precipitation over south Louisiana is negligible. Rather, Mississippi/Atchafalaya River discharge is driven by the integrated runoff throughout the much larger Mississippi River drainage basin that spans most of the conterminous United States as well as portions of Saskatchewan and Alberta, CA (inset, Fig. 1a).

2.2. Data sources

Hourly salinity data at 223 stations spanning 2010–2020 were obtained from the Coastwide Reference Monitoring System (CRMS; www.lacoast.gov/crms; Folse et al., 2020). Only stations for which <5% of the hourly values were missing and the longest consecutive gap <2 months during this 11-year period were included in the analysis (see Supplementary Table S2 for a list of stations used, including each station's overall data completeness and longest consecutive data gap). Each station's hourly salinity time series was aggregated into monthly averages, after which its monthly climatology was removed to provide a 223-station by 132-month matrix of monthly salinity anomalies $\boldsymbol{S}$. Gridded monthly precipitation data from the Parameter-Elevation Regressions on Independent Slopes Model (PRISM) dataset (Daly et al., 2008; www.prism.oregonstate.edu) were spatially averaged across the region bounded by 29.0°–30.5°N and 94.0° - 89.0°W (see Fig. 1, dashed box) to provide a monthly local precipitation anomaly time series across the Louisiana coastal zone. Daily Mississippi River discharge data collected at Tarbert Landing, Mississippi (www.rivergages.com), for the period 1950–2020 were aggregated to monthly averages, after which its

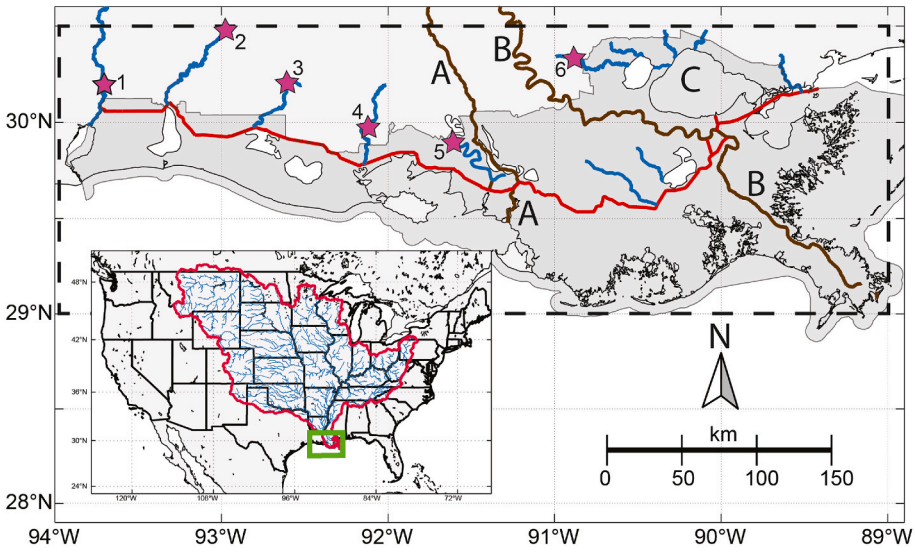

Fig. 1. Map of study area. The coastal zone, throughout which the 223 salinity monitoring stations are distributed, is shaded in dark gray. The Atchafalaya (A) and Mississippi (B) Rivers are shown by the brown lines. Smaller rivers, through which runoff from local precipitation enters the coastal zone, are shown in blue, including the Sabine R. (1), Calcasieu R. (2), Mermentau R. (3), Vermillion R. (4), Bayou Teche (5), and Amite R. (6). River gauging stations are shown by the purple stars. The Gulf Intracoastal Waterway is shown by the red line. Lake Pontchartrain is indicated by the letter C. The dashed box represents the region (29–30.5°N, 89–94°W) over which local precipitation was calculated. The inset is the location of the study area (green box), and the Mississippi River drainage basin, shown by the pink polygon. (For interpretation of the references to colour in this figure legend, the reader is referred to the Web version of this article.)

monthly climatology was removed to provide a time series of monthly discharge anomalies. Annual (Oct–Sep) precipitation anomalies across the conterminous United States derived from the PRISM dataset were related to seasonal-averaged values of the El Niño - Southern Oscillation (ENSO; Nino3.4; DJF) and North Atlantic Oscillation (NAO; Lisbon – Reykjavik; DJFM) indices (www.climatedataguide.ucar.edu/climate-data). Nino3.4 and NAO time series were normalized by their respective standard deviations, each calculated over the period 1950–2020.

2.3. Data analysis

Empirical orthogonal function (EOF) analysis (von Storch and Zwiers, 1999; Thompson and Emery, 2014) was applied to the 223 site x 132- month matrix $\boldsymbol{S}$ of salinity anomalies to identify its dominant modes of variability. EOF analysis optimally partitions the variance of a time-varying field into orthogonal patterns or modes by solving the eigenvalue problem for the covariance matrix of $\boldsymbol{S}$. Mathematically speaking, EOF analysis is identical to principal components analysis (PCA), with the only distinction being that the samples are ordered in time. The number of modes produced by the analysis is equal to the number of time series in $\boldsymbol{S}$ (223 in this case). Each mode is composed of an eigenvector that describes the spatial pattern, an eigenvalue that is proportional to the mode's contribution to the total variance in $\boldsymbol{S}$, and a time series (principal component; PC) that describes the EOF mode's evolution through time. The resulting PC time series of the leading modes can then be related to other geophysical time series to link these dominant modes of variability of the salinity field to specific forcing agents. EOF solutions were normalized to the standard deviations of their respective PCs, giving each PC time series a non-dimensional variance of unity (because salinity was measured using the Practical Salinity Scale, the eigenvectors are unitless as well). The percentage of local variance (i.e., the interannual salinity variance *at each site*) represented by each EOF mode was calculated as

$$p_{m,s} = 100 \times \lambda_m e_{m,s}^2 \Big/ \sigma_s^2$$

where λ_m is the eigenvalue of mode m, $e_{m,s}$ is the eigenvector element for mode m at site s, and σ_s^2 is the salinity variance at site s (it can also be obtained by taking the coefficient of determination that results from regressing the salinity anomaly time series at site s against the principal component time series of mode m). The local variance explained can show pronounced spatial structures (Janssen et al., 1999) and can thus be important for robust interpretation of the EOFs. The significance ($\alpha = 0.05$) of each of the resulting EOF modes was assessed with a Monte Carlo approach (10,000 simulations) applied to synthetic datasets of red noise each having autocorrelation functions identical to those in the salinity dataset, following Peng and Fyfe (1996). To assess the 95% significance level (r_{95}) for correlations among geophysical (e.g., precipitation, river discharge), climate index, and PC time series, correlation coefficients (r) were calculated for 10,000 pairs of randomly generated time series each having identical autocorrelation functions as the time series in question, and r_{95} was taken as the 95th percentile of the 10,000 correlation coefficients generated.

Composite analysis was used to investigate the spatial distribution of annual precipitation anomalies associated with different Nino3.4 and NAO phases across the conterminous United States. Years when the normalized climate index in question was $>0.5\sigma$ (σ = standard deviation) were grouped into the positive phase ensemble; years when the normalized climate index was $< -0.5\sigma$ were grouped into the negative phase ensemble. Composites for each climate index phase were then calculated by taking the mean annual precipitation value for each PRISM grid cell across the years selected for the climate index phase. Composite differences were then computed by subtracting the negative phase composite from the positive phase composite, and statistical significance of the composite differences in each grid cell was assessed with a Monte Carlo approach (Garcia-Herrera et al., 2006), where two separate groups of years were selected without repetition from all 71 years (1950–2020). The size of each group was set equal to the number of years that comprise each of the two composites, accounting for autocorrelation in the precipitation time series using $N_{eff} = N\ [(1 - r_1)/(1 + r_1)]$ (Bretherton et al., 1999), where r_1 is the lag-1 autocorrelation of the monthly precipitation time series for each grid cell of the PRISM dataset. The mean precipitation anomaly in each group and the difference between each group was calculated, and this procedure was repeated 5,000 times in each grid cell to obtain stable Gaussian probability density distributions. The observed difference in each grid cell was compared to the cell's 5,000 simulated differences, and if it was greater than the 95th percentile or less than the 5th percentile of the simulated differences then the observed difference was considered statistically significant ($p < 0.10$) for the grid cell. All maps presented herein were produced with Matlab version 9.10 (www.mathworks.com), using the M-map toolbox (version 1.4; www.eoas.ubc.ca/~rich/map.html).

3. Results

Mean annual salinity during 2010–2020 varied widely across the 223 sites from around 0.1 to greater than 20, with the highest salinities concentrated around the lower (seaward) reaches of the MRDP (Fig. 2a).

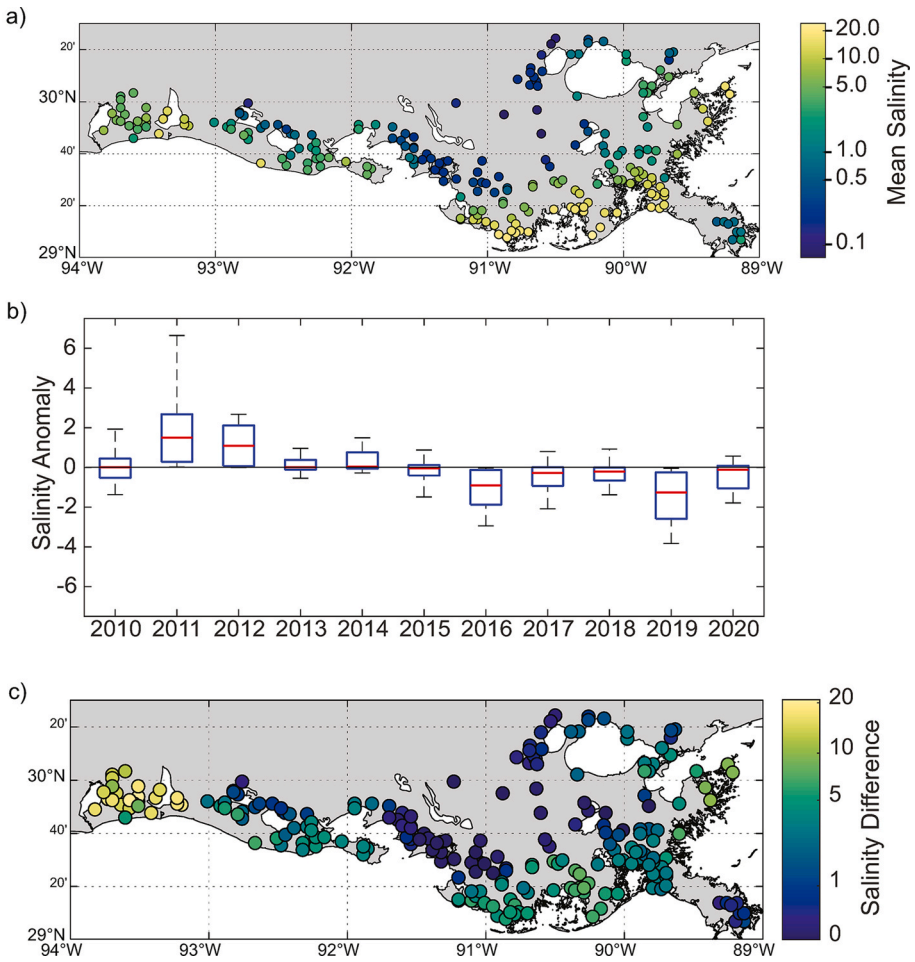

Fig. 2. Spatio-temporal interannual variability at 223 salinity monitoring sites 2010–2020. (a) Mean salinity at each of the 223 salinity monitoring sites 2010–2020. (b) Median (red lines) salinity anomaly, by year, for the 223 salinity monitoring sites, with interquartile range (blue box) and 5th and 95th percentiles (black whiskers). (c) Difference between 2011 and 2019 mean annual salinity at each site (positive indicates salinity $_{2011}$ > salinity $_{2019}$). (For interpretation of the references to colour in this figure legend, the reader is referred to the Web version of this article.)

The lowest salinities were found in the inland reaches of the MRDP and also near the mouth of the Atchafalaya River. Salinity anomalies were generally positive during the first half of the study period (Fig. 2b). The positive anomalies peaked in 2011 and then transitioned to negative anomalies by 2016. The negative anomalies persisted for the remainder of the study, with the largest negative anomalies occurring in 2019. Average annual salinities in 2011 exceeded those in 2019 by roughly 10 at the western sites, by roughly 5 in the lower MRDP, and by 0.1–3 near the mouths of the Mississippi and Atchafalaya Rivers and in the interior regions of the MRDP (Fig. 2c).

The first two EOF modes account for 85% of the total variance of the salinity field, and their eigenvalues exceeded the 95% significance thresholds generated by the Monte Carlo simulations (Fig. S1). None of the remaining EOF modes were significant. EOF1, which comprises 72% of the variance, carries the same sign (positive) across all stations, with markedly elevated loadings in the westernmost stations (Fig. 3a). Thus, this mode captures a spatial pattern in which salinity varies in-phase across the Louisiana coastal zone, with larger fluctuations in the LCP region of the study area. The principal component time series of this mode (PC_1; Fig. 3b) was strongly positive during 2011, after which it gradually declined to negative values. PC_1 was anticorrelated with the local precipitation anomaly ($r = -0.80$ [$r_{95} = -0.69$]; Fig. 3b) and lagged precipitation by 4–5 months, though this time lag may not be significant considering the 18-month filter applied to the time series (correlations at 0–3 month lags were also significant). Together, these findings suggest that negative local precipitation anomalies are associated with positive salinity anomalies throughout coastal Louisiana, and that salinity is particularly responsive to local precipitation anomalies in the western part of the state where the EOF1 loadings are relatively large. This mode explains most of the local variance at the westernmost sites and also at sites along the western rim of Lake Pontchartrain, but it captures relatively little of the local variance at sites near the mouths of the Mississippi and Atchafalaya Rivers (Fig. 3c).

The annual (Oct–Sep) local precipitation anomaly is positively correlated with the Nino3.4 index (DJF) from 1950 to 2020 ($r = 0.67$ [$r_{95} = 0.20$]; Fig. 3d). The strong El Niño events of 1957–1958, 1966, 1973, 1982–1983, 1991, 1997, 2002–2004 and 2015 are coincident with (± 1 yr) local precipitation surpluses. Similarly, the strong La Niña events of 1962, 1988–1989, 1999–2000, and 2011 all co-occur with local precipitation deficits. Composite analysis of PRISM precipitation anomalies with respect to ENSO phase corroborates this correlation, showing positive anomalies during positive ENSO phase years across the southeastern United States, including coastal Louisiana, where the composite differences were in the range of +20–40 cm yr^{-1} (Fig. 3e). Thus, positive (negative) ENSO phases are associated with positive (negative) local precipitation anomalies and negative (positive) salinity anomalies across Louisiana's entire coastal wetland landscape.

EOF2 comprised 13% of the variance in the salinity field and exhibited a dipole pattern, whereby the loadings tended to be positive for the eastern stations (MRDP) and negative on the western side (LCP; Fig. 4a). PC_2 was anticorrelated with Mississippi River discharge anomaly (Fig. 4b; $r = -0.72$ [$r_{95} = -0.61$]) and lagged discharge by 1–2 months. Thus. positive river discharge anomalies were associated with reduced salinities on the eastern side of the state and elevated salinities on the western side. Up to 60% of the local salinity variance is captured by EOF2 at sites near the mouth of the Mississippi River and throughout the lower MRDP; the importance of this mode diminishes with increasing distance inland in this region (Fig. 4c). EOF2 captures only a

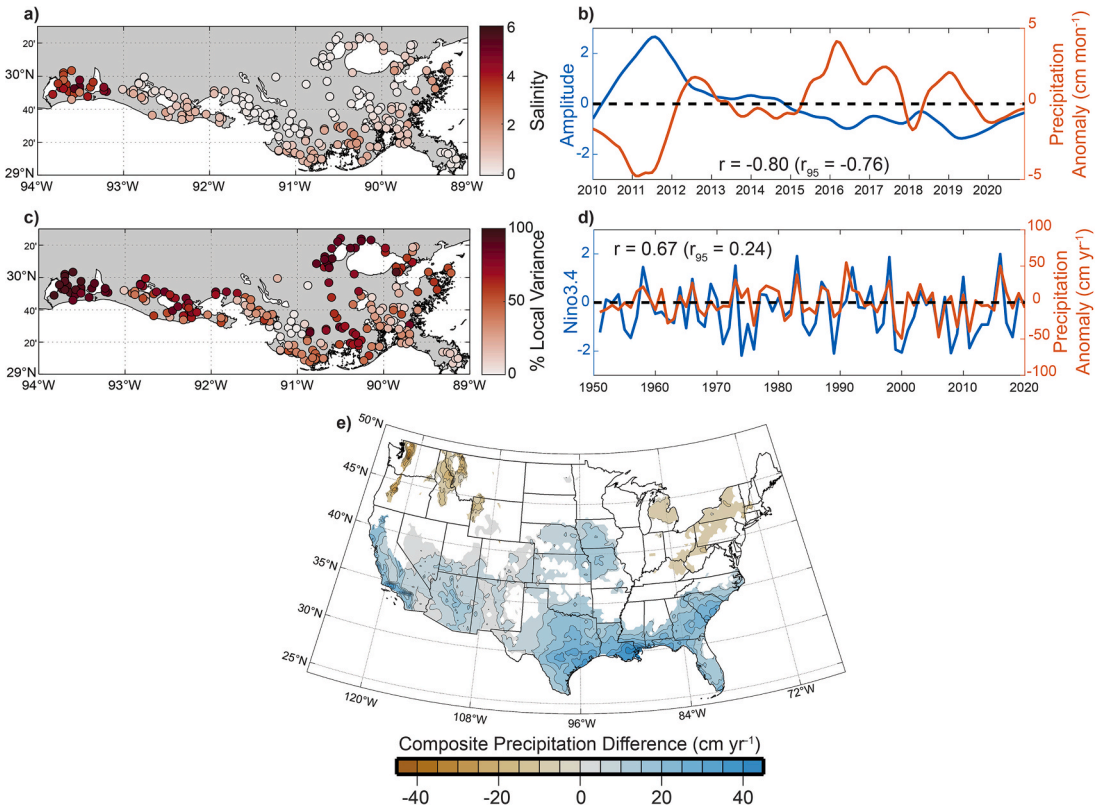

Fig. 3. (a) Eigenvector loadings for the first mode (EOF1), obtained through EOF analysis of 2010–2020 monthly salinity anomalies at 223 salinity monitoring sites; (b) amplitude of principal component time series for EOF1 (blue); local precipitation anomaly (orange) - both time series have been smoothed with a 18-month Lowess filter; (c) percent local variance explained by EOF1; (d) normalized Niño3.4 time series (blue); local precipitation anomaly (orange); (e) composite precipitation difference (positive minus negative) with respect to Niño3.4 phase. Only regions where composite precipitation difference was significant ($\alpha = 0.10$) are shown. (For interpretation of the references to colour in this figure legend, the reader is referred to the Web version of this article.)

small portion of local variance for most sites in the LCP (west of 92°W). Thus, while the negative EOF2 loadings are prominent outside the MRDP, they appear to be inconsequential to the overall interannual salinity variability in this region.

Mississippi River discharge anomaly, which was shown above to be inversely correlated with PC2, is positively correlated with the NAO index from 1950 to 2020 (Fig. 4d). Peak correlation occurs when discharge anomaly lags NAO by one year ($r = 0.35$ [$r_{95} = 0.22$]). Composite analysis of PRISM precipitation anomalies with respect to NAO phase shows positive precipitation anomalies throughout much of the Mississippi River drainage basin during years following positive NAO phase (i.e., accounting for the one-year precipitation lag; Fig. 4e). Thus, positive (negative) NAO phases are associated with positive (negative) precipitation anomalies across the Mississippi River drainage basin during the following year, which drive positive (negative) Mississippi River discharge anomalies. When these discharge anomalies are positive, salinity in the lower Mississippi River delta is reduced and salinity at many of the sites in southwest Louisiana increases.

4. Discussion

Salinity across Louisiana's coastal wetlands shows considerable interannual variation that has been linked to ENSO and NAO through teleconnections with local and Mississippi River basin-scale precipitation variability. The amplitude of these variations is higher in the western (LCP) region of the state (Fig. 2c), where salinity differences between the 2011 La Niña and 2019 El Niño events approach 10. The higher variation in this region of the study site may reflect the LCP's restricted estuary-ocean exchange that would otherwise flush the region during droughts and promote retention of local runoff during wet years.

Two modes of variability together account for 85% of the interannual salinity variation across Louisiana's coastal wetlands. The first EOF mode (a large effect impacting the entire Louisiana coastal zone) captures a pattern whereby salinity varies in-phase across coastal Louisiana, with the amplitude of these salinity fluctuations being quite large in the far western regions of the study area (Fig. 3). Temporally, this pattern is correlated with local precipitation variability ($r = -0.80$) under the influence of ENSO, where positive (negative) local precipitation anomalies are associated with El Niño (La Niña) conditions ($r = 0.67$) and tend to decrease (increase) salinity across coastal Louisiana. The larger eigenvector loadings at the far western sites is consistent with previous findings of low-frequency salinity fluctuations in this region being highly sensitive to local precipitation anomalies due to restricted estuary-ocean exchange in the region (McGinnis and Aucoin, 2015). Prior investigations have observed correspondence between precipitation anomalies and ENSO phase in the southeastern United States, whereby during El Niño (La Niña) phases the subtropical jet stream intensifies (weakens), increasing (decreasing) cyclogenesis (Ropelewski and Halpert, 1986; Schmidt et al., 2001; McCabe and Muller, 2002) and moisture flux from the Pacific (Sanchez-Rubio et al., 2011). This ENSO/southeastern U.S. precipitation teleconnection and its impact on coastal salinity has been identified as a driver of brown shrimp abundance (Piazza et al., 2010) and oyster disease-induced mortality (Soniat et al., 2009) in the MRDP. Those findings are corroborated here and suggest the ENSO/brown shrimp teleconnection may extend beyond the MRDP to all of coastal Louisiana.

Positive (negative) Mississippi River discharge anomalies are associated with positive (negative) NAO phases ($r = 0.35$), through the NAO's influence on precipitation anomalies throughout a broad region of the Mississippi River drainage basin, and tend to decrease (increase)

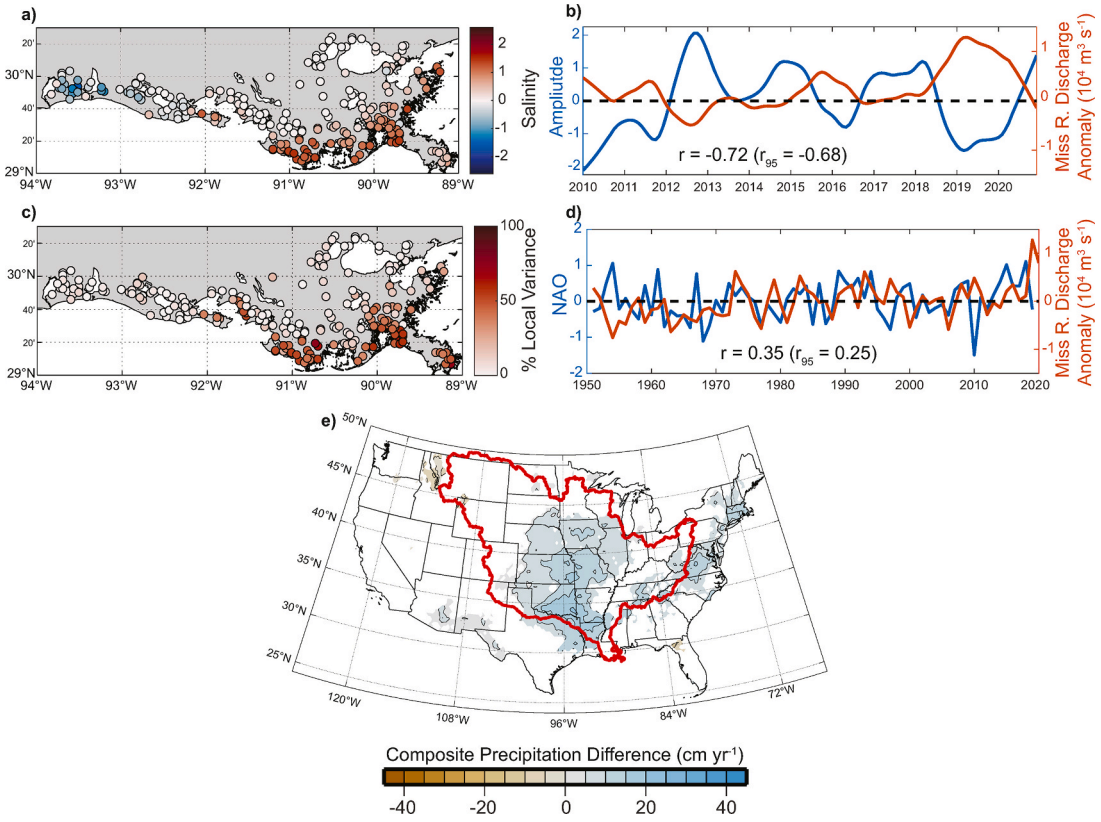

Fig. 4. (a) Eigenvector loadings for the second mode (EOF2), obtained through EOF analysis of 2010–2020 monthly salinity anomalies at 223 salinity monitoring sites; (b) amplitude of principal component time series for EOF2 (blue); Mississippi River discharge anomaly (orange) - both time series have been smoothed with a 18-month Lowess filter; (c) percent local variance explained by EOF2; (d) normalized NAO time series (blue); Mississippi River discharge anomaly (orange); (e) composite precipitation difference (positive minus negative) with respect to NAO phase. Only regions where composite precipitation difference was significant ($\alpha = 0.10$) are shown. The Mississippi River drainage basin boundary is indicated by red line. (For interpretation of the references to colour in this figure legend, the reader is referred to the Web version of this article.)

salinity near the mouths of the Mississippi and Atchafalaya Rivers and in the lower MRDP (with little to no impact elsewhere in the study area; Fig. 4). Elevated Mississippi River discharge has been associated with positive NAO phases (Sanchez-Rubio et al., 2011), and similar streamflow-NAO relations have been observed throughout the central Mississippi River basin tributary network (Tootle et al., 2005). During positive NAO phases, the Bermuda High intensifies, resulting in stronger trade winds and enhanced evaporation across the Caribbean and GOM (Wallace et al., 1990). As these moisture-laden trade winds turn northward along the northern GOM margin, they inject moisture over the central Mississippi River drainage basin (Helfand and Schubert, 1995). Using tree-ring data as a proxy for precipitation, this correspondence between the NAO and central North American precipitation over sub-decadal timescales has been observed going back to the mid-1600s (Fye et al., 2006). The NAO-Mississippi River discharge correlation ($r = 0.35$) is considerably weaker than the Nino3.4-local precipitation correlation ($r = 0.67$), possibly because (1) there exist expansive regions of the Mississippi River drainage basin that lie beyond the extent of the NAO/precipitation action center (Fig. 4e), (2) reservoir operations in the basin designed for water storage and flood control can decouple precipitation and river discharge, or (3) this teleconnection is modulated to some degree by other, longer-period climate modes that have also been linked to Mississippi River discharge (such as the Atlantic Multidecadal Oscillation; Enfield et al., 2001).

The spatial patterns of EOF2 eigenvector loadings (Fig. 4a) and local variance explained (Fig. 4c) on the MRDP, which carry large values at the seaward reaches and diminish landward, are strongly suggestive of the coastal ocean as a source of freshwater. West of the Mississippi River's mouth, freshwater discharged onto the shelf flows westward alongshelf as a stratified coastal current (Chew et al., 1962; Cochrane and Kelly, 1986; Schroeder et al., 1987). During river flood events, this buoyant coastal current can act to reverse the horizontal density gradient between the shelf and the bays of the lower MRDP, inducing negative estuarine flows such that plume waters on the shelf flow into the MRDP bays through the tidal passes (Juarez et al., 2020), and these freshwater intrusion events have been observed in time-series of satellite imagery (Payandeh et al., 2021). These dynamics have also been identified with numerical modeling spanning much of the same time period as this study (2012–2018; Ou et al., 2020).

Loadings for EOF2 exhibited a dipole pattern, where they were negative for many of the LCP sites in western Louisiana, and hence opposite those on the distal reaches of the MRDP on the eastern side of the study area (Fig. 4b). This dipole spatial pattern suggests that unlike most of the MRDP sites where positive river discharge anomalies were associated with reduced salinity, at many of the LCP sites they were counterintuitively associated with elevated salinities. This dipole pattern may simply be an artifact of the orthogonality constraint of EOF analysis, which forces the scalar product between EOF1 and higher modes to zero (Navarra and Simonici, 2010) and can consequently promote a domain-wide dipole pattern in EOF2 when the dominant mode (EOF1) carries the same sign throughout the domain (Houghton and Tourre, 1992; Dommenget and Latif, 2002; Lian and Chen, 2012). If no reason exists for the physical processes driving the system to exhibit orthonormal conditions (e.g., if the correlation coefficient between the local precipitation and Mississippi River discharge anomaly time series is not exactly zero), some of the dynamics beyond those captured in the dominant first mode can remain obscured in combinations of the higher modes. Regardless of the origin of the negative EOF2 loadings in the

western region of the study area, the local variance explained by EOF2 in this region was very low, possibly due to reduced estuary-ocean exchange and associated estuarine flushing with relatively fresh Mississippi River plume waters in the LCP region (relative to the MRDP region) of the Louisiana coastal zone (McGinnis and Aucoin, 2015). As a result, interannual salinity variation across the LCP region of the study area could be overwhelmingly attributed to the local precipitation/ENSO mode (EOF1).

Salinity sensors in the CRMS network became operational 2006–2008, and data which meet completeness criteria spanning >200 sites go back to 2010. As such, the CRMS salinity data analyzed in this study (2010–2020) span a single ENSO cycle. Thus, the local precipitation/EOF1 and Mississippi River discharge/EOF2 linkages identified here are tenuous and their persistence should be further examined as new CRMS salinity data become available. Linkages between climate modes (Nino3.4, NAO) and precipitation, on the other hand, are based on several decades of data (1950–2020) and corroborate previous findings (Schmidt et al., 2001; McCabe and Muller, 2002; Sanchez-Rubio et al., 2011).

Indices of Earth's internal climate modes such as ENSO and NAO are becoming increasingly predictable. For example, increases in warm water volume in the equatorial Pacific generally precede the onset of El Niño conditions by eight months (McPhaden, 2003), and persistent, multi-year La Niña conditions often follow years with very strong El Niño events (Iwakiri and Wantanabe, 2021). Likewise, robust and skillful predictions of wintertime (DJF) NAO can be made from sea-ice concentration, stratospheric circulation, and sea-surface temperature conditions during the preceding autumn (Wang et al., 2017). The quasi-predictability of these climate indices suggests that prevailing estuarine salinity conditions in Louisiana may be anticipated several months to a few years in advance, allowing for management measures such as regulation of freshwater inflows or design of oyster reef restoration networks (Swam et al., 2022) to have elements of proactivity rather than being strictly reactive endeavors.

Ecological restoration efforts in the northern GOM wetlands have been central to managing these ecosystems for the last 30 years (LCWCRTF, 1998), and investment in these efforts has accelerated since the Deepwater Horizon incident in 2010 (CPRA, 2017). Many of these restoration measures, such as Mississippi River diversions, will convey large influxes of freshwater to their estuarine receiving basins in attempt to stimulate deltaic land building with fluvial sediments (Allison and Meselhe, 2010). Given that maximum suspended sediment concentrations occur during river flood events (Mossa, 1996; Snedden et al., 2007), it has been recommended that diversion operations be coincident with river floods (Peyronnin et al., 2017). Under this approach large freshwater inflows occurring mid-estuary via river diversions would be coincident with large influxes of freshwater from plume waters on the shelf, which together may impose dual freshening influences throughout the lower and middle reaches of their estuarine basins. These dynamics have been confirmed with numerical models (Ou et al., 2020), which indicate substantial salinity reductions in the lower MRDP in response to operations of a proposed river diversion. This basin-scale freshening may have implications for estuarine fisheries distribution and productivity. More generally, successful restoration planning and implementation requires an understanding of how salinity is impacted by cyclical climate variability, and that restoration monitoring data be interpreted within the context of this variability. The teleconnections between cyclical climate variability and salinity identified here clearly illustrate the importance of their incorporation into monitoring and modeling efforts to assess or predict restoration impacts, and to inform uncertainty about those predictions. The background climate variability, once known, may be constrained by integrating appropriate explanatory variables into statistical and numerical models, allowing for restoration impacts to be better resolved.

These findings can inform expectations regarding how salinity regimes in coastal Louisiana will be impacted by anticipated changes in climate and land use in the coming decades. Continued sea-level rise will have the tendency to increase saltwater intrusion throughout coastal Louisiana, as it has in a multitude of other estuaries throughout the world (Ross et al., 2015; Yang et al., 2015; van Maanen and Sottolichio, 2018; Vu et al., 2018). Though total annual precipitation in the southeastern United States is expected to remain unchanged throughout the next several decades (Hayhoe et al., 2018), interannual variation in total precipitation in the region has increased over the last 70 years and this increased variability has been associated with warming sea surface temperatures in the Atlantic (Wang et al., 2010; Li et al., 2011). If this increasing trend of precipitation variability in the region is a manifestation of the secular warming trend over the observational record, it may continue into the future. Taken together, these circumstances – continued sea-level rise and increased year-to-year local precipitation variability – point to increased salinities throughout coastal Louisiana in the coming decades with larger interannual fluctuations, particularly in the western region where the local precipitation effect (EOF1) is most pronounced. These impacts may be mitigated to some degree in the lower MRDP where the Mississippi River discharge effect (EOF2) was most prominent, given that Mississippi River discharge is projected to increase by 10–60% by the 2090s over that observed in the 2000s, depending on climate, atmospheric CO_2, and land-use change scenarios (Tao et al., 2014).

Recent research has explored the possibility of scaling up oyster fishery planning and management efforts from single site- or reef-level to entire estuarine basins, and defining oyster production zones based on maps of mean salinity over recent years (Swam et al., 2022). Findings here may provide context for those efforts, particularly if production zones are defined based on biased salinity records spanning only a portion of the ENSO cycle. Similarly, marsh vegetation community zonation (fresh, intermediate, brackish, saline) has been assessed throughout coastal Louisiana via end-of-season aerial surveys conducted at roughly decadal recurrence intervals over the last 25 years (Visser et al., 1998, 2000, 2002; Sasser et al., 2008, 2014; Nyman et al., 2022). The first four surveys all occurred after marked precipitation deficits (Fig. 4d), while the last occurred shortly after a precipitation surplus had persisted for three years. These findings suggest that decadal-interval vegetation mapping may be aliasing the ENSO signal and that higher-frequency (i.e., annual) mapping efforts (e.g., based on remote sensing imagery) may be needed to disentangle cyclical variations associated with internal climate variability from long-term trends associated with restoration activities and climate change.

CRediT authorship contribution statement

Gregg A. Snedden: Writing – review & editing, Writing – original draft, Formal analysis, Conceptualization.

Declaration of competing interest

The authors declare that they have no known competing financial interests or personal relationships that could have appeared to influence the work reported in this paper.

Data availability

All datasets used in this study are publicly available and online links to all datasets have been provided in the manuscript text.

Acknowledgements

Support and funding were provided by the U.S. Geological Survey Ecosystems Mission Area and the Coastal Wetlands Planning, Protection and Restoration Act, Coastwide Reference Monitoring System. Robert Twilley and Megan La Peyre provided constructive comments to a previous version of this manuscript. Any use of trade, firm, or product

names is for descriptive purposes only and does not imply endorsement by the U.S. Government.

Appendix A. Supplementary data

Supplementary data to this article can be found online at https://doi.org/10.1016/j.ecss.2023.108487.

References

Allison, M.A., Meselhe, E.A., 2010. The use of large water and sediment diversions in the lower Mississippi River (Louisiana) for coastal restoration. J. Hydrol. 387, 346–360.

Baustian, M.M., Stagg, C.L., Perry, C.L., Moss, L.C., Carruthers, T.J.B., Allison, M., 2017. Relationships between salinity and short-term soil carbon accumulation rates from marsh types across a landscape in the Mississippi River delta. Wetlands 37, 313–324.

Baustian, M.M., Stagg, C.L., Perry, C.L., Moss, L.C., Carruthers, T.J.B., 2021. Long-term carbon sinks in marsh soils of coastal Louisiana are at risk to wetland loss. J. Geophys. Res.: Biogeosciences 126, e2020JG005832, 2021.

Bitencourt, L.P., Fernandes, E., Möller, O., Ross, L., 2020. The contribution of ENSO cycles to the salinity spatio-temporal variability in a bar-built microtidal estuary. Regional Studies in Marine Science 40, 101496.

Bretherton, C.S., Widmann, M., Dymnikov, V.P., Wallace, J.M., Bladé, I., 1999. The effective number of spatial degrees of freedom of a time-varying field. J. Clim. 12, 1990–2009.

Byrne, J.V., LeRoy, D.O., Riley, C.M., 1959. The Chenier Plain and its Stratigraphy, Southwestern Louisiana, vol. 9. Transaction of the Gulf Coast Association of Geological Societies, pp. 237–260.

Chew, F., Drennan, K.L., Demoran, W.J., 1962. Some results of drift bottle studies off the Mississippi delta. Limnol. Oceanogr. 7, 252–257.

Cloern, J.E., Abreu, P.C., Carstensen, J., Chauvaud, L., Elmgren, R., Grall, J., Greening, H., Johansson, J.O.R., Kahru, M., Sherwood, E.T., Xu, J., Kedong, Y., 2016. Human activities and climate variability drive fast-paced change across the world's estuarine-coastal ecosystems. Global Change Biol. 22, 513–529.

Cochrane, J.D., Kelly, F.J., 1986. Low-frequency circulation on the Texas-Louisiana continental shelf. J. Geophys. Res.: Oceans 91, 10645–10659.

Couvillion, B.R., Beck, H., Schoolmaster, D., Fischer, M., 2017. Land Area Change in Coastal Louisiana (1932 to 2016), vol. 3381. U.S. Geological Survey Scientific Investigations Map.

Daly, C., Halbleib, M., Smith, J.I., Gibson, W.P., Doggett, M.K., Taylor, G.H., Curtis, J., Pasteris, P.P., 2008. Physiographically sensitive mapping of climatological temperature and precipitation across the conterminous United States. Int. J. Climatol. 28, 2031–2064.

de Miranda, L.B., de Castro, B.M., Kjerfve, B., 1998. Circulation and mixing due to tidal forcing in the Bertioga Channel, São Paulo, Brazil. Estuaries 21, 204–214.

DeMarco, K., Couvillion, B., Brown, S., La Peyre, M., 2018. Submerged aquatic vegetation mapping in coastal Louisiana through development of a spatial likelihood occurrence (SLOO) model. Aquat. Bot. 151, 87–97.

Dommenget, D., Latif, M., 2002. A cautionary note on the interpretation of EOFs. J. Clim. 15, 216–225.

Dong, L., Su, J., Deng, J., Chen, Qi, 2007. The importance of estuarine gravitational circulation on the early life of the Bohai Penaeid prawn. J. Mar. Syst. 67, 253–262.

Enfield, D.B., Mestas-Nuñez, A.M., Trimble, P.J., 2001. The Atlantic Multidecadal Oscillation and its relation to rainfall and river flows in the continental U.S. Geophys. Res. Lett. 28, 2077–2080.

Fernandes, E.H.L., Dyer, K.R., Moller, O.O., Niencheski, L.F.H., 2002. The Patos Lagoon hydrodynamics during an El Niño event (1998). Continent. Shelf Res. 22, 1699–1713, 2002.

Folse, T.M., McGinnis, T.E., Sharp, L.A., West, J.L., Hymel, M.K., Troutman, J.P., Weifenbach, D., Boshart, W.M., Rodrigue, L.B., Richardi, D.C., Wood, W.B., Miller, C. M., Robinson, E.M., Freeman, A.M., Stagg, C.L., Couvillion, B.R., Beck, H.J., 2020. A Standard Operating Procedures Manual for the Coastwide Reference Monitoring System-*Wetlands* and the System-wide Assessment and Monitoring Program: Methods for Site Establishment, Data Collection, and Quality Assurance/quality Control. Louisiana Coastal Protection and Restoration Authority, p. 252.

Fye, F.K., Stahle, D.W., Cook, E.R., Cleaveland, M.K., 2006. NAO influence on sub-decadal moisture variability over central North America. Geophys. Res. Lett. 33, L15707.

Garcia, A.M., Viera, J.P., Winemiller, K.O., 2001. Dynamics of the shallow-water fish assemblage of the Patos Lagoon estuary (Brazil) during cold and warm ENSO episodes. J. Fish. Biol. 59, 1218–1238.

Garcia-Herrera, R., Calvo, N., Garcia, R.R., Giorgetta, M.A., 2006. Propagation of ENSO temperature signals into the middle atmosphere: a comparison of two general circulation models and ERA-40 reanalysis data. J. Geophys. Res. Atmos. 111, D06101.

Garvine, R.W., 1985. A simple model of estuarine subtidal fluctuations forced by local and remote wind stress. J. Geophys. Res.: Oceans 90, 11945–11948.

Gould, H.R., McFarlan, E., 1959. Geologic history of the Chenier Plain, southwestern Louisiana. Trans. Gulf Coast Assoc. Geol. Soc. 9, 261–270.

Helfand, H.M., Schubert, S.D., 1995. Climatology of the simulated Great Plains low-level jet and its contribution to the continental moisture budget of the United States. J. Clim. 8, 784–806.

Herrera, D., Cunniff, S., DuPont, C., Cohen, B., Gangi, D., Kar, D., Snider, N.P., Rojas, V., Wyerman, J., Norriss, J., Mounternot, M., 2019. Designing an environmental impact bond for wetland restoration in Louisiana. Ecosyst. Serv. 35, 260–276.

Hilton, T.W., Jajjar, R.G., Zhong, L., Li, M., 2008. Is there a signal of sea-level rise in Chesapeake Bay salinity? J. Geophys. Res.: Oceans 113, C09002.

Houghton, R.W., Tourre, Y.M., 1992. Characteristics of low-frequency sea surface temperature fluctuations in the tropical Atlantic. J. Clim. 5, 765–772.

Howarth, R., Chan, F., Conley, D.J., Garnier, J., Doney, S.C., Marino, R., Billen, G., 2011. Coupled biogeochemical cycles: eutrophication and hypoxia in temperate estuaries and coastal marine ecosystems. Front. Ecol. Environ. 9, 18–26.

Iwakiri, T., Wantanabe, M., 2021. Mechanisms linking multi-year La Niña with preceding strong El Niño. Sci. Rep. 11, 17465.

Janousek, C.N., Dugger, B.D., Drucker, B.M., Thorne, K.M., 2020. Salinity and inundation effects on productivity of brackish tidal marsh plants in the San Francisco Bay-Delta Estuary. Hydrobiologia 847, 4311–4323.

Janssen, F., Schrum, C., Backhaus, J.O., 1999. A climatological data set of temperature and salinity for the Baltic Sea and the North Sea. Dtsch. Hydrogr. Z. 51, 5.

Juarez, B., Valle-Levinson, A., Li, C., 2020. Estuarine salt-plug induced by freshwater pulses from the inner shelf. Estuarine. Coastal and Shelf Science 232, 106491.

La Peyre, M.K., Geaghan, J., Decossas, G., La Peyre, J.E., 2016. Analysis of environmental factors influencing salinity patterns, oyster growth, and mortality in lower Breton Sound Estuary, Louisiana, using 20 years of data. J. Coast Res. 32, 519–530.

Laska, S., Wooddell, G., Hagelman, R., Grambling, R., Farris, M.T., 2005. At risk: the human, community and infrastructure resources of coastal Louisiana. J. Coast Res. 44, 90–111.

Latham, P.J., Pearlstine, L.G., Kitchens, W.M., 1994. Species association changes across a gradient of freshwater, oligohaline, and mesohaline tidal marshes along the lower Savannah River. Wetlands 14, 174–183.

LCWCRTF (Louisiana Coastal Wetlands Conservation and Restoration Task Force), 1998. Coast 2050: toward a Sustainable Coastal Louisiana. Louisiana Department of Natural Resources, p. 161.

Lerczak, J.A., Geyer, W.R., Chant, R.J., 2006. Mechanisms driving the time-dependent salt flux in a partially stratified estuary. J. Phys. Oceanogr. 36, 2296–2311.

Li, W., Li, L., Fu, R., Deng, Y., Wang, H., 2011. Changes to the north Atlantic Subtropical High and its role in the intensification of summer rainfall variability in the southeastern United States. J. Clim. 24, 1499–1506.

Lian, T., Chen, D., 2012. An evaluation of rotated EOF analysis and its application to tropical Pacific SST variability. J. Clim. 25, 5361–5373.

MacCready, P., Geyer, W.R., 2001. Estuarine salt flux through an isohaline surface. J. Geophys. Res.: Oceans 106, 11629–11637.

Mace, M.M., Rozas, L.P., 2017. Population dynamics and secondary production of juvenile white shrimp (*Litopenaeus setiferus*) along an estuarine salinity gradient. Fish. Bull. 115, 74–88.

Maes, J., van Damme, P.A., Taillieu, A., Ollevier, F., 1998. Fish communities along an oxygen-poor salinity gradient (Zeeschelde Estuary, Belguium). J. Fish. Biol. 52, 534–546.

Malone, T.C., Crocker, L.H., Pike, S.E., Wendler, B.W., 1988. Influences of river flow on the dynamics of phytoplankton production in a partially stratified estuary. Mar. Ecol. Prog. Ser. 48, 235–249.

McCabe, G.J., Muller, R.A., 2002. Effects of ENSO on weather-type frequencies and properties at New Orleans, Louisiana, USA. Clim. Res. 20, 95–105.

McGinnis, T., Aucoin, S., 2015. Operations, maintenance, and monitoring report for east mud lake marsh management (CS-20). Coastal protection and restoration authority of Louisiana. Operations – Lafayette Regional Office. Lafayette, Louisiana. 46pp.

McKee, K.L., Mendelssohn, I.A., Materne, M.D., 2004. Acute salt marsh dieback in the Mississippi River deltaic plain: a drought-induced phenomenon? Global Ecol. Biogeogr. 13, 65–73.

McPhaden, M.J., 2003. Tropical Pacific Ocean heat content variations and ENSO persistence barriers. Geophys. Res. Lett. 30, 33.

Meerhoff, E., Tapia, F.J., Sobarzo, M., Castro, L., 2015. Influence of estuarine and secondary circulation on crustacean larval fluxes: a case study from a Patagonian fjord. J. Plankton Res. 37, 168–182.

Mize, S.V., Demcheck, D.K., 2009. Water quality and phytoplankton communities in Lake Pontchartrain during and after the bonnet carré spillway opening, april to october 2008, in Louisiana, USA. Geo Mar. Lett. 281, 431–440.

Morris, A.W., Mantoura, R.F.C., Bale, A.J., Howland, R.J.M., 1978. Very low salinity regions of estuaries: important sites for chemical and biological reactions. Nature 274, 678–680.

Mossa, J., 1996. Sediment dynamics in the lowermost Mississippi River. Engineering Geologoy 45, 457–479.

Murphy, R.R., Kemp, W.M., Ball, W.P., 2011. Long-term trends in Chesapeake Bay seasonal hypoxia, stratification, and nutrient loading. Estuar. Coast 34, 1293–1309.

Navarra, A., Simonici, V., 2010. A Guide to Empirical Orthogonal Functions for Climate Data Analysis. Springer, Dordrecht, p. 151pp.

Norcross, B.L., Shaw, R.F., 1984. Ocean and estuarine transport of fish eggs and larvae: a review. Trans. Am. Fish. Soc. 113, 153–165.

Nowicki, B.L., 1994. The effect of temperature, oxygen, salinity, and nutrient enrichment on estuarine denitrification rates measured with a modified nitrogen gas flux technique. Estuar. Coast Shelf Sci. 38, 137–156.

Nyman, J.A., Reid, C.S., Sasser, C.E., Linscombe, J., Hartley, S.B., Couvillion, B.R., Villani, R.K., 2022. Vegetation Types in Coastal Louisiana in 2021. U.S. Geological Survey Data Release. https://doi.org/10.5066/P9URYLMS.

Ou, Y., Xue, Z.G., Li, C., Xu, K., White, J.R., Bentley, S.J., Zang, Z., 2020. A numerical investigation of salinity variations in the Barataria Estuary, Louisiana in connection with the Mississippi River and restoration activities. Estuar. Coast Shelf Sci. 245, 107021.

Payandeh, A.R., Justic, D., Mariotti, G., Huang, H., Valentine, K., Walker, N.D., 2021. Suspended sediment dynamics in a deltaic estuary controlled by subtidal motion and offshore river plumes. Estuarine. Coastal and Shelf Science 250, 107137.
Peng, S., Fyfe, J., 1996. The coupled patterns between sea level pressure and sea surface temperature in the midlatitude north Atlantic. J. Clim. 9, 1824–1839.
Peyronnin, N., Green, M., Richards, C.P., Owens, A., Reed, D., Chamberlain, J., Groves, D.G., Rhinehart, W.K., Belhadjali, K., 2013. Louisiana's 2012 Coastal Master Plan: overview of a science-based and publicly informed decision-making process. J. Coast Res. 67, 1–15.
Peyronnin, N.S., Caffey, R.H., Cowan, J.C., Justic, D., Kolker, A.S., Laska, S.B., McCorquodale, A., Melancon, E., Nyman, J.A., Twilley, R.R., Visser, J.M., White, J. R., Wilkins, J.G., 2017. Optimizing sediment diversion operations: working group recommendations for integrating complex ecological and social landscape interactions. Water 9, 368.
Piazza, B.P., La Peyre, M.K., Keim, B.D., 2010. Relating large-scale climate variability to local species abundance: ENSO forcing and shrimp in Breton Sound, Louisiana, USA. Clim. Res. 42, 195–207.
Ralston, D.K., Geyer, W.R., Lerczak, J.A., 2008. Subtidal salinity and velocity in the Hudson river estuary: observations and modeling. J. Phys. Oceanogr. 38, 753–770.
Ralston, D.K., Geyer, W.R., Lerczak, J.A., 2010. Structure, variability, and salt flux in a strongly forced salt wedge estuary. J. Geophys. Res.: Oceans 115, C06005.
Ropelewski, C.F., Halpert, M.S., 1986. North American precipitation and temperature patterns associated with the El Niño/Southern Oscillation (ENSO). Mon. Weather Rev. 114, 2352–2362.
Ross, A.C., Najjar, R.G., Li, M., Mann, M.E., Ford, S.E., Katz, B., 2015. Sea-level rise and other influences on decadal-scale salinity variability in a coastal plain estuary. Estuar. Coast Shelf Sci. 157, 79–92.
Rozas, L.P., Minello, T.J., 2011. Variation in penaeid shrimp growth rates along an estuarine salinity gradient: implications for managing river diversions. J. Exp. Mar. Biol. Ecol. 397, 196–207.
Sanchez-Rubio, G., Perry, H.M., Biesiot, P.M., Johnson, D.R., Lipcius, R.N., 2011. Oceanic-atmospheric modes of variability and their influence on riverine input to coastal Louisiana and Mississippi. J. Hydrol. 396, 72–78.
Sanford, L.P., Boicourt, W.C., 1990. Wind-forced salt intrusion into a tributary estuary. J. Geophys. Res.: Oceans 95, 13357–13371.
Sasser, C.E., Visser, J.M., Mouton, E., Linscombe, J., Hartley, S.B., 2008. Vegetation types in coastal Louisiana in 2007. In: U.S. Geological Survey Open-File Report 2008-1224.
Sasser, C.E., Visser, J.M., Mouton, E., Linscombe, J., Hartley, S.B., 2014. Vegetation Types in Coastal Louisiana in 2013, vol. 3290. U.S. Geological Survey Scientific Investigations Map.
Schmidt, N., Luther, M.E., 2002. ENSO impacts on salinity in Tampa Bay, Florida. Estuaries 25, 976–984.
Schmidt, N., Lipp, E.K., Rose, J.B., Luther, M.E., 2001. ENSO influences on seasonal rainfall and river discharge in Florida. J. Clim. 14, 615–628.
Schroeder, W.W., Dinnel, S.P., Wiseman, W.J., Merrell, W.J., 1987. Circulation patterns inferred from the movement of detached buoys in the eastern Gulf of Mexico. Continent. Shelf Res. 7, 883–894.
Seo, D.C., Yu, K., Delaune, R.D., 2008. Influence of salinity level on sediment denitrification in a Louisiana estuary receiving diverted Mississippi River Water. Arch. Agron Soil Sci. 54, 249–257.
Snedden, G.A., 2019. Patterning emergent marsh vegetation assemblages in coastal Louisiana, USA, with unsupervised artificial neural networks. Appl. Veg. Sci. 22, 213–229.
Snedden, G.A., Cable, J.E., Swarzenski, C., Swenson, E., 2007. Sediment discharge into a subsiding Louisiana deltaic estuary through a Mississippi River diversion. Estuar. Coast Shelf Sci. 71, 181–193.
Snedden, G.A., Cretini, K., Patton, B., 2015. Inundation and salinity impacts to above- and belowground productivity in *Spartina patens* and *Spartina alterniflora* in the Mississippi River deltaic plain: implications for using river diversions as restoration tools. Ecol. Eng. 81, 133–139.
Soniat, T.M., Hofmann, E.E., Klinck, J.M., Powell, E.N., 2009. Differential modulation of eastern oyster (*Crassostrea virginica*) disease parasites by the el-niño-southern oscillation and the North Atlantic oscillation. Int. J. Earth Sci. 98, 99–114.
Spalding, E.A., Hester, M.W., 2007. Interactive effects of hydrology and salinity on oligohaline plant species productivity: implications of relative sea-level rise. Estuar. Coast 30, 214–225.
Steadman, S., Dahl, T.E., 2008. Status and Trends of Wetlands in the Coastal Watersheds of the Eastern United States 1998 to 2004. National Oceanic and Atmospheric Administration. National Marine Fisheries Service and U.S. Department of Interior, Fish and Wildlife Service, pp. 1–32.
Stenseth, N.C., Mysterud, A., Ottersen, G., Hurrell, J.W., Chan, K.S., Lima, M., 2002. Ecological effects of climate fluctuations. Science 297, 1292–1296.
Steyer, G.D., Sasser, C.E., Visser, J.M., Swenson, E.M., Nyman, J.A., Raynie, R.C., 2003. A proposed coast-wide reference monitoring system for evaluating wetland restoration trajectories in Louisiana. Environ. Monit. Assess. 81, 107–117.
Swam, L.M., Couvillion, B., Callam, B., La Peyre, J.F., La Peyre, M.K., 2022. Defining oyster resource zones across coastal Louisiana for restoration and aquaculture. Ocean Coast Manag. 225, 106178.
Swarzenski, C.M., 2003. Surface Water Hydrology of the Gulf Intracoastal Waterway in South-Central Louisiana, 1996-1999. U.S. Geological Survey Professional Paper 1672.
Tao, B., Tian, H., Ren, W., Yang, J., Yang, Q., He, R., Cai, W., Lohrenz, S., 2014. Increasing Mississippi River discharge throughout the 21st century influenced by changes in climate, land use, and atmospheric CO_2. Geophys. Res. Lett. 41, 4978–4986.
Telesh, I., Schubert, H., Skarlato, S., 2013. Life in the salinity gradient: discovering mechanisms behind a new biodiversity pattern. Estuar. Coast Shelf Sci. 135, 317–327.
Thompson, R.E., Emery, W.J., 2014. Data Analysis Methods in Physical Oceanography. Elsevier, p. 716.
Tolan, J.M., 2007. El Niño-Southern Oscillation impacts translated to the watershed scale: estuarine salinity patterns along the Texas Gulf Coast, 1982-2004. Estuarine. Coastal and Shelf Science 72, 247–260.
Tominack, S.A., Coffey, K.Z., Yoskowitz, D., Sutton, G., Wetz, M.S., 2020. An assessment of trends in the frequency and duration of *Karenia brevis* red tide blooms on the south Texas coast (western Gulf of Mexico). PLoS One 15, e0239309.
Tootle, G.A., Piechota, T.C., Singh, A., 2005. Coupled oceanic atmospheric variability and U.S. streamflow. Water Resour. Res. 41, W12408.
van de Broek, M., Temmerman, S., Merckx, R., Govers, G., 2016. Controls on soil organic carbon stocks in tidal marshes along an estuarine salinity gradient. Biogeosciences 13, 6611–6624.
van der Molen, J.S., Perissinotto, R., 2011. Microalgal productivity in an estuarine lake during a drought cycle: the St. Lucia Estuary, South Africa. Estuarine. Coastal and Shelf Science 92, 1–9.
van Maanen, B., Sottolichio, A., 2018. Hydro- and sediment dynamics in the Gironde estuary (France): sensitivity to seasonal variations in river inflow and sea level rise. Continent. Shelf Res. 165, 37–50.
Visser, J.M., Sasser, C.E., Chabreck, R.H., Linscombe, R.G., 1998. Marsh vegetation types of the Mississippi River deltaic plain. Estuaries 21, 818–828.
Visser, J.M., Sasser, C.E., Linscombe, R.G., Chabreck, R.H., 2000. Marsh vegetation types of the Chenier Plain. Louisiana. Estuaries 23, 318–327.
Visser, J.M., Sasser, C.E., Chabreck, R.H., Linscombe, R.G., 2002. The impact of a severe drought on the vegetation of a subtropical estuary. Estuaries 25, 1184–1195.
von Storch, H., Zwiers, F.W., 1999. Statistical Analysis in Climate Research. Cambridge University Press, p. 484.
Vu, D.T., Yamada, T., Ishidaira, H., 2018. Assessing the impact for sea level rise due to climate change on seawater intrusion in the Mekong Delta, Vietnam. Water Sci. Technol. 77, 1632–1639.
Wallace, J.M., Smith, C., Jiang, Q., 1990. Spatial patterns of atmosphere-ocean interaction in the northern winter. J. Clim. 3, 990–998.
Wang, H., Fu, R., Kumar, A., Li, W., 2010. Intensification of summer rainfall variability in the southeastern United States during recent decades. J. Hydrometeorol. 11, 1007–1018.
Wang, L., Ting, M., Kushner, P.J., 2017. A robust empirical seasonal prediction of winter NAO and surface climate. Sci. Rep. 7, 279.
Wang, H., Gilbert, J.A., Zhu, Y., Yang, X., 2018. Salinity is a key factor driving the nitrogen cycling in the mangrove sediment. Sci. Total Environ. 631–632, 1342–1349.
Wei, X., Schramkowski, G.P., Schuttelaars, H.M., 2016. Salt dynamics in well-mixed estuaries: importance of advection by tides. J. Phys. Oceanogr. 46, 1457–1475.
Whitney, M.M., 2010. A study on river discharge and salinity variability in the middle atlantic bight and long Island Sound. Continent. Shelf Res. 30, 305–318.
Wilber, D.H., 1992. Associations between freshwater inflows and oyster productivity in Apalachicola Bay, Florida. Estuar. Coast Shelf Sci. 35, 179–199.
Willis, J.M., Hester, M.W., 2004. Interactive effects of salinity, flooding, and soil type on *Panicum hemitomon*. Wetlands 24, 43–50.
Winder, M., Sommer, U., 2012. Phytoplankton response to a changing climate. Hydrobiologia 698, 5–16.
Wong, K.C., 1995. On the relationship between long-term salinity variations and river discharge in the middle reach of the Delaware estuary. J. Geophys. Res.: Oceans 100, 20705–20713.
Wong, K.C., Moses-Hall, J.E., 1998. On the relative importance of the remote and local wind effects to the subtidal variability in a coastal plain estuary. J. Geophys. Res.: Oceans 103, 18393–18404.
Xu, Y., Hoitink, A.J.F., Zheng, J., Kästner, K., Zhang, W., 2019. Analytical model captures intratidal variation in salinity in a convergent, well-mixed estuary. Hydrol. Earth Syst. Sci. 23, 4309–4322.
Yang, Z., Wang, T., Voisin, N., Copping, A., 2015. Estuarine response to river flow and sea-level rise under future climate change and human development. Estuar. Coast Shelf Sci. 156, 19–30.